Pharmaceutical Research, Vol. 22, No. 1, January 2005 (© 2005)
DOI: 10.1007/s11095-004-9013-3

Research Paper

Functional Evidence for P-glycoprotein at the Nose-Brain Barrier

Candace L. Graff[1] and Gary M. Pollack[1,2]

Received July 22, 2004; accepted September 17, 2004

Purpose. Experiments were performed to assess the brain distribution of [^{3}H]-verapamil, including the influence of delivery route of inhibitor and substrate (nasal vs. systemic) on brain distribution. The anatomic location of P-glycoprotein (P-gp) at the nose-brain barrier also was investigated.
Methods. Separate groups of mice were pretreated with rifampin or vehicle nasally or intravenously. [^{3}H]-verapamil was administered either nasally or via *in situ* brain perfusion, and dose-response profiles were constructed for P-gp inhibition. Localization of P-gp in freshly obtained brain slices and olfactory tissue was evaluated by confocal microscopy.
Results. Rifampin inhibited the P-gp–mediated efflux of [^{3}H]-verapamil, regardless of delivery route ($I_{max} = 62 \pm 6\%$). The ED_{50} for enhancement of [^{3}H]-verapamil uptake by nasal rifampin was ~400-fold lower than for intravenous rifampin (0.16 vs. 65 mg/kg, respectively). Microscopy showed that P-gp was located in endothelial cells that line the olfactory bulb and within the olfactory epithelium.
Conclusions. Nasal delivery of rifampin enhanced brain uptake of [^{3}H]-verapamil. The magnitude of transport inhibition was dependent on the dose and route of the inhibitor, the time after administration of the inhibitor, and the specific brain region examined. P-gp is localized to both the olfactory epithelium and the endothelial cells that surround the olfactory bulb.

KEY WORDS: brain slices; blood-brain barrier; nasal delivery; P-glycoprotein; pharmacokinetics.

INTRODUCTION

Central nervous system (CNS) diseases remain difficult to treat due to poor brain penetration of therapeutic agents. The primary limitation of uptake of these agents is the blood-brain barrier (BBB). The BBB consists of polarized endothelial cells connected by tight junctions that limit paracellular permeability (1). Various methods have been evaluated to improve BBB penetration and thereby increase brain uptake. These methods have included increasing substrate lipophilicity (to increase passive permeability), increasing carrier-mediated transport across the BBB by conjugation with a substrate of an endogenous uptake transporter (2), and decreasing efflux through transport inhibition or chemical modification of the substrate. In addition, nasal delivery has been explored as a means to deliver substrates to the CNS. However, this approach has found limited utility. While some substrates can be delivered directly to the brain via this route, the efficiency of brain uptake is dependent on the substrate, and many of the mechanisms governing this process are not well understood. Previous work has shown that efflux transporters attenuate brain uptake of substrates after nasal administration, and that this attenuation can be overcome by nasal administration of appropriate transport inhibitors (3). These observations seem to suggest that an analogue of the BBB, including relevant uptake and efflux transport systems, is operative at this site

The localization of P-glycoprotein (P-gp) at the nose-brain interface, which would result in attenuation of brain uptake of substrates, remains in question. It has been demonstrated that the olfactory receptor neurons that lie within the olfactory epithelium in *Xenopus laevis* tadpoles express P-gp (4), and Kandimalla and Donovan recently showed the presence and function of P-gp in excised bovine olfactory epithelium (5). P-gp also is expressed in normal human nasal mucosa (6). In addition, the *mdr1a* isoform of P-gp has been shown to be present in the olfactory bulb of naïve rats via reverse transcriptase polymerase chain reaction (RT-PCR) (7). Thus, it seems likely that P-gp located at the olfactory epithelium, as well as within the olfactory bulb itself, operates to limit the uptake of nasally administered substrates into the murine brain.

There have been numerous efforts to inhibit P-gp at the BBB to improve substrate penetration. However, the results of these attempts have been mostly disappointing. Given that P-gp is present throughout the body and usually plays a protective role, indiscriminately inhibiting this transporter could lead to adverse drug interactions. In addition, overlapping substrate specificity between CYP3A4 and P-gp means that many inhibitors can affect both proteins, leading to unintended drug interactions (8). While the brain is very sensitive to P-gp inhibition, the placenta appears to be sensitive as well (9), which could pose problems with drug-induced teratogenicity. Hepatic and intestinal P-gp can be affected by inhibitors as well, which would lead to a decrease in both intestinal and biliary excretion of compounds, resulting in

[1] Division of Drug Delivery and Disposition, School of Pharmacy, University of North Carolina, Chapel Hill, North Carolina 27599, USA.
[2] To whom correspondence should be addressed. (e-mail: gary_pollack@unc.edu)

increased absorption and decreased elimination (10). P-gp also is located in the myocardium, and P-gp inhibition has been shown to lead to increased accumulation of digoxin in cardiac tissue (11).

In contrast, nasal delivery may represent a promising alternative to systemically delivered P-gp inhibitors. For instance, the inhibitor could be administered nasally to target the BBB, with the pharmacologic substrate administered systemically. Efflux transporters such as P-gp represent significant barriers to effective delivery of pharmacologic agents to the brain. The ability to deliver modulators of P-gp or other transporters specifically to the brain or the BBB, thus avoiding interactions with transport proteins in other organs and tissues, would represent a significant advantage in delivering therapeutic agents to the CNS. This paper addresses the efficacy of nasally administered rifampin, a model P-gp inhibitor, in increasing brain uptake of the model P-gp substrate [^{3}H]-verapamil. In addition, experiments were performed to evaluate the caudal distribution of [^{3}H]-verapamil, and the dependence of distribution on the delivery route of both inhibitor and substrate (nasal vs. systemic). Finally, this study evaluated the anatomic location of P-gp operating at the nose-brain interface.

MATERIALS AND METHODS

Materials

Probe substrates were obtained from the following sources: [^{3}H]-(±)-verapamil (85 Ci/mmol) (NEN Life Science Products, Boston, MA, USA); rifampin (Spectrum, New Brunswick, NJ, USA); (±)-verapamil hydrochloride (Sigma-Aldrich, St. Louis, MO, USA). Polyclonal antibodies were obtained from the following sources: Glut1 and pan-cytokeratin (Santa Cruz Biotech., Santa Cruz, CA, USA); C219 (Signet Laboratories, Dedham, MA, USA); mouse IgG2a/FITC (Alexis Biochemicals, San Diego, CA, USA); anti-goat IgG antibodies (molecular probes, Eugene, OR, USA). All other chemicals and reagents were of the highest grade available from commercial sources.

Animals

Adult CF-1 mice [*mdr1a*(–/–) and *mdr1a*(+/+), 30–45 g] were purchased from Charles River Laboratories, Inc. (Wilmington, MA, USA) and maintained in a breeding colony in the School of Pharmacy, The University of North Carolina (Chapel Hill, NC, USA). Animals were housed in a temperature- and humidity-controlled room with a 12-h light/dark cycle and had free access to food and water. The experimental protocol was approved by the Institutional Animal Care and Use Committee of the University of North Carolina. All experimental procedures were conducted according to the Guide for the Care and Use of Laboratory Animals (Institute of Laboratory Animal Resources, Commission on Life Sciences, National Research Council, Washington, DC, 1996).

Nasal Administration

Mice (n = 4) were anesthetized with intraperitoneal (i.p.) ketamine/xylazine (140/8 mg/kg). Mice were placed in a supine position with a dowel (~7 mm) placed under the neck to limit liquid flow down the trachea. Solutions containing test compounds (37°C) were gassed with 95% O_2 and 5% CO_2 for pH control (7.4) prior to instillation. When appropriate, radiolabeled tracers (2 μCi/ml; 0.5 mCi/ml for slicing experiments) were added. Solutions were administered via separate 10-μl gas-tight syringes (2-inch, 23-G needle) to each nostril. Timing of the experiment was initiated following completion of instillation.

In situ Brain Perfusion

The details of *in situ* mouse perfusion have been described elsewhere (12). Briefly, mice (n = 4) were anesthetized as described above. A catheter (polyethylene tubing, 0.30 mm i.d. × 0.70 mm o.d.) was placed in the left common carotid artery after ligation of the external branch. The cardiac ventricles were severed immediately before brain perfusion with Krebs-bicarbonate buffer via a syringe pump (60 s, 2.5 ml/min, pH 7.4 with 95% O_2 and 5% CO_2, 37°C) containing 1 μM [^{3}H]-verapamil (0.1 μCi/ml). [^{14}C]-inulin (0.3 μCi/ml) was added as a vascular space marker. The perfusion was terminated by decapitation; the brain was dissected on ice and the left hemisphere (~140 mg) and perfusate (~150 mg) were collected and weighed in tared 8-ml glass scintillation vials. Brain tissue was digested with 0.7 ml of Solvable (Packard, Boston, MA) at 50°C overnight. Samples were vortex-mixed with 5 ml of scintillation cocktail (Ultimate Gold XR; Packard). Total radioactivity (^{3}H and ^{14}C) was determined simultaneously in a PerkinElmer 1600TR liquid scintillation analyzer. Brain samples obtained from naïve mice were analyzed, and these blank samples were subtracted from all analyzed samples to correct for apparent background.

Influence of Route of Administration of Inhibitor and Substrate on Brain Uptake

For the group (n = 4) that received both inhibitor and substrate nasally, rifampin (5 μl; 0.30 μg/kg to 0.27 mg/kg) was administered to each nostril of P-gp-competent mice as described above. Control animals received only methanol vehicle (in preliminary studies, brain uptake of [^{3}H]-verapamil was similar in the presence vs. the absence of methanol), and P-gp-deficient animals were included to define complete inhibition of P-gp–mediated transport. After 7 min, 2.5 μl aliquots of saline containing [^{3}H]-verapamil (5 μM; 2 μCi) were administered to each nostril, and the experiment was terminated 3 min later via decapitation. The brain was excised and total radioactivity was determined as described in the Materials and Methods.

For the group (n = 4) that received the inhibitor nasally and substrate systemically, rifampin (5 μl; 0.30 μg/kg to 0.27 mg/kg) was administered to each nostril of P-gp–competent mice as described above. Immediately following the instillation of rifampin, the mice were prepared for *in situ* brain perfusion, and the perfusion was initiated 35 min following the nasal instillation of rifampin. This time point was selected because 35 min is the minimum time necessary to prepare the animal for the *in situ* brain perfusion. The *in situ* brain perfusion was performed and samples were analyzed as described above.

For the group (n = 4) that received the inhibitor systemically and substrate nasally, rifampin (25–150 mg/kg; i.v.) was administered via tail vein injection (<0.30 ml/animal).

Thirty-five min after rifampin administration, 2.5 μl aliquots of saline containing [^{3}H]-verapamil (5 μM; 2 μCi) were administered to each nostril. The experiment was terminated 3 min later and the samples were processed and analyzed as above.

For the group (n = 4) that received both the inhibitor and substrate systemically, rifampin (25–150 mg/kg, i.v.) was administered via tail vein injection (<0.30 ml/animal). Immediately following the administration of rifampin, the mice were prepared for *in situ* brain perfusion and the perfusion was initiated 35 min following the nasal instillation of rifampin. The *in situ* brain perfusion was performed and samples were analyzed as described above.

Determination of Total Radioactivity

Tissue samples were digested in Solvable (Packard) at 50°C overnight (1 ml for whole brain, 0.7 ml for a single hemisphere). After cooling, Ultima Gold XR (Packard) scintillation cocktail was added (15 ml for whole brain, 5 ml for a single hemisphere), and the sample was vortex-mixed. Scintillation counting (referenced to appropriate quench curves for single- or dual-label counting, depending on the experiment) was performed in a Packard Tri-Carb model 1900 TR (Packard). Brain samples obtained from naïve mice were analyzed, and these blank samples were subtracted from all analyzed samples to correct for apparent background.

Calculation of BBB Transport Parameters

Parameters related to the *in situ* brain perfusion were calculated based on the method described by Smith (13). Brain vascular volume (V_{vasc}, ml/100 g) was estimated from tissue distribution of [^{14}C]-inulin, which is known to diffuse very slowly across the BBB, according to the following equation:

$$V_{vasc} = \frac{X^*}{C^*}$$

where X* and C* represent [^{14}C]-inulin in the brain (dpm/100 g) and perfusate (dpm/ml), respectively. Apparent brain distributional volumes of substrates (V_{brain}, ml/100 g) were calculated as according to the following equation:

$$V_{brain} = \frac{X_{brain}}{C_{perf}}$$

where X_{brain} is substrate in the brain (dpm/100 g) corrected for vascular contamination ($X_{total} - [V_{vasc} \cdot C_{perf}]$) and C_{perf} is substrate concentration in perfusate (dpm/ml). Initial uptake clearance of substrates (Cl_{up}, ml/100 g/min) were calculated as follows:

$$Cl_{up} = \frac{X_{brain}/T}{C_{perf}}$$

where T is the perfusion time (min).

Fresh Tissue Slicing

For each of the experimental groups described above, an additional group (n = 3) was included to allow examination of [^{3}H]-verapamil disposition. These experiments were performed exactly as above, except that the specific activity of [^{3}H]-verapamil was increased to 0.5 mCi/ml in order to increase the limit of detection. At the end of each set of experiments, the brain was dissected on ice, blotted dry and mounted on a platform with cyanoacrylate to allow for coronal slicing. After allowing the tissue to set for approximately 2 min, the platform was submersed in 2°C phosphate buffered saline (PBS) to allow for slicing (Vibratome 3000; Vibratome, St. Louis, MO, USA); 300-micron thick sections were cut (in a rostral-to-caudal direction) with 35°-blade angle using Vibratome feather blades [low speed (1), high amplitude (8)]. Slices were removed from the buffer bath and placed in tared 8-ml glass scintillation vials and weighed. The tissue was digested with 0.3 ml of Solvable (Packard) at 50°C overnight. Cooled samples were vortex-mixed with 5 ml of scintillation cocktail (Ultimate Gold XR; Packard), and total radioactivity was determined as described above.

Immunohistochemistry

After decapitation, the brains were removed rapidly and embedded in Tissue-Tek O.C.T. compound (Sakura, Torrance, CA, USA) and stored at −20°C until analysis. In addition, the majority of the olfactory turbinates (~35 mg of tissue) were removed, fixed (4% paraformaldehyde in PBS), decalcified (0.5 M EDTA at 4°C overnight), embedded in O.C.T. medium and stored at −20°C until cutting on the cryomicrotome. Frozen horizontal sections containing the olfactory bulb (20 μm) and serial coronal sections (20 μm) containing the olfactory epithelium were cut with a Leica CM1850 cryostat microtome (Leica, Bannockburn, IL, USA) at −15°C. The sections were thaw-mounted onto Superfrost Plus Micro Slides (VWR Scientific, West Chester, PA, USA). The samples were fixed in ice-cold acetone for 10 min at 4°C and allowed to air dry quickly. Samples were rinsed with ice-cold blocking buffer (0.01 M PBS containing 5% goat serum and 1% bovine serum albumin) three times. Blocking buffer was removed and samples were incubated immediately with anti-MDR1 (1:100, C219), anti-cytokeratin (1:100), and/or anti-Glut1 (1:100) primary antibodies using CoverWell imaging chamber gaskets (Molecular Probes, Eugene, OR, USA) for 5 h. Samples were washed 3× with 0.01 M PBS for 15 min and subsequently incubated with fluorochrome conjugated secondary antibodies using CoverWell imaging chamber gaskets for 90 min. Samples were washed again (3×) with 0.01 M PBS and rinsed briefly with distilled water. Glass cover slips were mounted onto the tissue using glycerol. Immunofluorescent images were detected using Zeiss LSM5 Pascal Laser Scanning Confocal Microscope (Microscopy Services Laboratory UNC-CH Department of Pathology & Laboratory Medicine) interfaced to an Optronics DEI 750 cooled CCD camera via an Apple Macintosh G3 computer system utilizing a Scion CG7 capture card. Confocal scanning was performed in the *x-y* field with a pinhole setting of 1.00 airy disk units. Laser power and PMT gain were held constant for each sample. Scan averaging was set to 8 and the 63x oil immersion objective lens was used for all image acquisitions.

Data Analysis

Data are presented as mean ± SD for n = 4 per group unless otherwise noted. Where appropriate, a two-tailed Student's *t* test was used to evaluate the statistical significance of

differences between experimental groups. In all cases, $p < 0.05$ was used as the criterion of statistical significance.

The degree of inhibition of P-gp–mediated efflux of [^{3}H]-verapamil for the nasal experiments was calculated using the following formula:

$$\% \text{ inhibition} = \frac{DPM_{rifampin} - DPM_{vehicle}}{DPM_{mdr1a(-/-)} - DPM_{vehicle}} \times 100$$

where $DPM_{rifampin}$ is the total radioactivity in rifampin-treated *mdr1a(+/+)* mice, and the $DPM_{vehicle}$ and $DPM_{mdr1a(-/-)}$, are the total radioactivity in vehicle-treated *mdr1a(+/+)* and *mdr1a(–/–)* mice, respectively. Likewise, the degree of inhibition of P-gp–mediated efflux of [^{3}H]-verapamil for the *in situ* brain perfusion studies was defined as follows:

$$\% \text{ inhibition} = \frac{Cl_{up,mdr1a(+/+)} - Cl_{up,mdr1a(+/+),vehicle}}{Cl_{up,mdr1a(-/-),vehicle} - Cl_{up,mdr1a(+/+),vehicle}} \times 100$$

where $Cl_{up,mdr1a(+/+)}$ is the initial uptake clearance of [^{3}H]-verapamil in rifampin-treated *mdr1a*(+/+) mice, and $Cl_{up,mdr1a(+/+),\ vehicle}$ and $Cl_{up,mdr1a(-/-),\ vehicle}$ are the initial uptake clearance of [^{3}H]-verapamil in vehicle-treated *mdr1a*(+/+) and *mdr1a*(–/–) mice, respectively. The concentration-dependent inhibition of P-gp–mediated [^{3}H]-verapamil efflux data were analyzed by nonlinear least-squares regression (WinNonlin 3.2; Pharsight, Mountain View, CA, USA) to obtain estimates of key parameters (E_{max}, ED_{50}, γ). Appropriate statistical and model selection criteria were used to evaluate model performance. Assessment of the goodness of fit of the model to the observed data was based on coefficients of variation (CV%) and distribution of residual error.

RESULTS

Brain Uptake Following Nasal Administration of Inhibitor

In order to elaborate fully the ability of nasally administered rifampin to inhibit P-gp–mediated flux, dose-response relationships were constructed for the influence of nasally administered rifampin on the brain uptake of [^{3}H]-verapamil. The relationship between transport inhibition of nasally administered [^{3}H]-verapamil and nasally administered rifampin dose(s) is shown in Fig. 1. The profile was characterized by an E_{max} of 99 ± 3% (i.e., essentially complete inhibition of P-gp–mediated transport of [^{3}H]-verapamil at administered rifampin concentrations approaching 1 mM), and an ED_{50} of 22 ± 2 μg/kg. For this study, there was no difference in % inhibition between waiting 7 min vs. 35 min between inhibitor and substrate administration.

The relationship between transport inhibition of systemically administered [^{3}H]-verapamil by nasally administered rifampin is shown in Fig. 2. The profile was associated with an E_{max} of 61 ± 19% and an ED_{50} of 170 ± 50 μg/kg. From this figure, it is apparent that maximum inhibition was not achieved. Due to limitations in the solubility of rifampin, 1 mM was the highest concentration achievable. Therefore, an additional experiment was performed to attempt to increase the amount of rifampin delivered nasally. To accomplish this, 10-μl aliquots (5 μl/nostril) of rifampin (0.27 mg/kg) were administered at 4 successive time points (0, 5, 10, and 15 min) to a group (n = 4) of animals prior to the *in situ* perfusion.

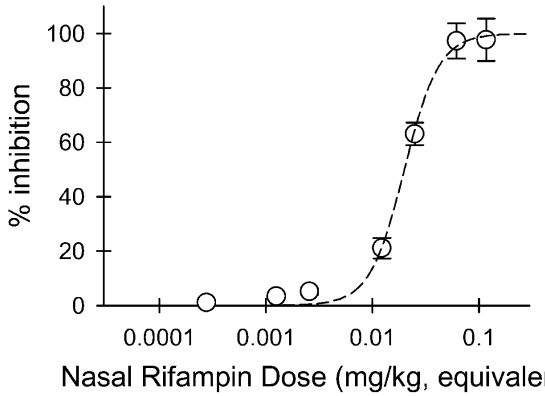

Fig. 1. Dose-response relationship for inhibition of P-gp–mediated efflux transport of nasally administered [^{3}H]-verapamil by nasally administered rifampin. Symbols represent mean ± SD for n = 4 per rifampin dose. The fitted line represents a sigmoidal Hill equation with E_{max} = 99 ± 3%, ED_{50} = 22 ± 2 μg/kg, γ = 2.7 ± 0.4 (parameter estimate ± standard error).

This method of nasal delivery increased the % inhibition achieved via this route from 44 ± 3% (at 0.27 mg/kg, equivalent) to 72 ± 4% (at 1 mg/kg, equivalent).

To serve as an additional control, rifampin was administered to *mdr1a(–/–)* mice to ensure that mechanisms other than P-gp inhibition did not enhance [^{3}H]-verapamil brain uptake. There was no statistical difference between the [^{3}H]-verapamil uptake in *mdr1a(–/–)* mice treated with rifampin vs. vehicle-treated animals for the nasal delivery of rifampin.

Brain Uptake Following Systemic Administration of Inhibitor

To more fully demonstrate the ability of rifampin to inhibit P-gp–mediated efflux of [^{3}H]-verapamil, dose-response profiles were constructed for the influence of systemically administered rifampin on the brain uptake of [^{3}H]-verapamil. The relationship between transport inhibition of systemically administered [^{3}H]-verapamil by systemically administered rifampin is shown in Fig. 3. The profile was associated with an E_{max} of 62 ± 9% and an ED_{50} of 65 ± 10 mg/kg.

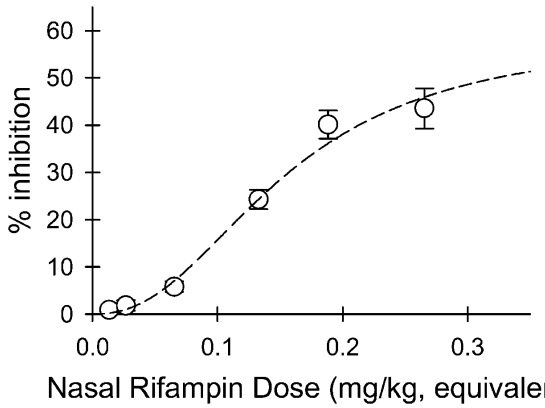

Fig. 2. Dose-response relationship for inhibition of P-gp–mediated efflux transport of systemically administered [^{3}H]-verapamil by nasally administered rifampin. Symbols represent mean ± SD for n = 4 per rifampin dose. The fitted line represents a sigmoidal Hill equation with E_{max} = 61 ± 19%, ED_{50} = 170 ± 50 μg/kg, γ = 2.2 ± 0.5 (parameter estimate ± standard error).

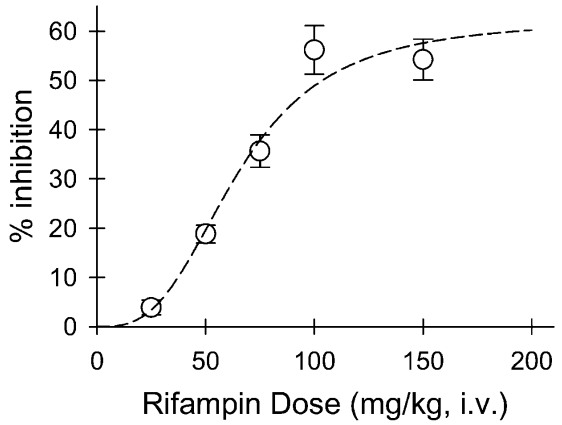

Fig. 3. Dose-response relationship for inhibition of P-gp–mediated efflux transport of systemically administered [^{3}H]-verapamil by systemically administered rifampin. Symbols represent mean ± SD for n = 4 per rifampin dose. The fitted line represents a sigmoidal Hill equation with E_{max} = 62 ± 9%, ED_{50} = 65 ± 10 mg/kg, γ = 3.0 ± 0.6 (parameter estimate ± standard error).

The relationship between transport inhibition of nasally administered [^{3}H]-verapamil by systemically delivered rifampin is shown in Fig. 4. Again, inhibition was incomplete (E_{max} = 75 ± 12%) and the ED_{50} (76 ± 9 mg/kg) was similar to that against systemic [^{3}H]-verapamil. As with the preceding experiment, there was no statistical difference between the [^{3}H]-verapamil uptake in *mdr1a(–/–)* mice treated with rifampin vs. vehicle-treated animals for the systemic delivery of rifampin.

Comparison of Nasally Administered and Systemically Administered Rifampin on the Ability to Enhance Brain Uptake of [^{3}H]-Verapamil

While both nasally administered and systemically administered rifampin were able to attenuate the P-gp–mediated efflux of [^{3}H]-verapamil, the doses administered between the two routes of administration differed greatly. Figure 5 depicts the simultaneous modeling of the % inhibition of P-gp–

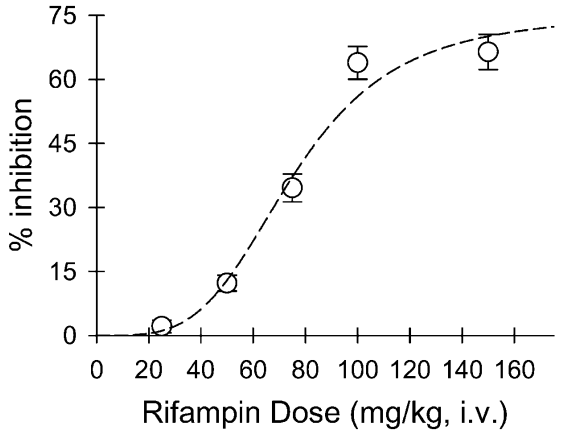

Fig. 4. Dose-response relationship for inhibition of P-gp–mediated efflux transport of nasally administered [^{3}H]-verapamil by systemically administered rifampin. Symbols represent mean ± SD for n = 4 per rifampin dose. The fitted line represents a sigmoidal Hill equation with E_{max} = 75 ± 12%, ED_{50} = 76 ± 9 mg/kg, γ = 3.8 ± 0.9 (parameter estimate ± standard error).

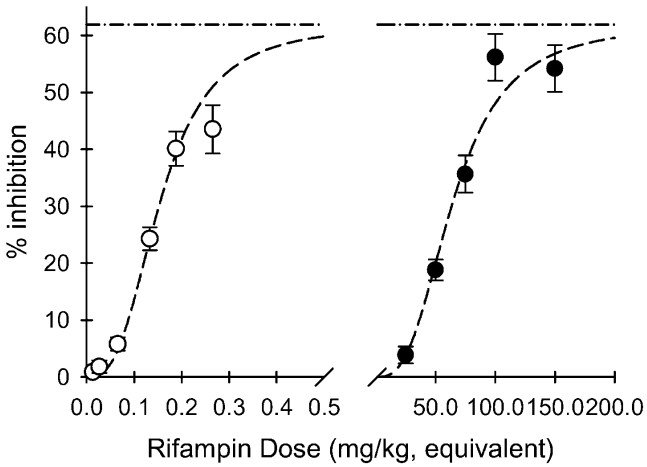

Fig. 5. Simultaneous modeling of the dose-response relationships for inhibition of P-gp–mediated efflux transport of systemically administered [^{3}H]-verapamil by nasally administered rifampin (○) vs. systemically administered rifampin (●). Symbols represent mean ± SD for n = 4 per rifampin dose. The fitted lines represents a sigmoidal Hill equation with E_{max} = 62 ± 6%, ED_{50} = 65 ± 7 mg/kg, γ = 2.9 ± 0.4, and a potency ratio of 417 ± 42 (parameter estimate ± standard error).

mediated efflux of systemically administered [^{3}H]-verapamil by nasally administered rifampin vs. systemically administered rifampin. The dose-dependent inhibition of P-gp–mediated [^{3}H]-verapamil efflux data were analyzed by nonlinear least-squares regression using a sigmoidal E_{max} model:

$$\%\ \text{Inhibition} = \frac{E_{max} \cdot \text{Dose}^{\gamma}}{\frac{ED_{50}^{\gamma}}{PR} + \text{Dose}^{\gamma}}$$

where E_{max} is the maximum percentage of inhibition of P-gp–mediated efflux by rifampin, dose is the administered Dose of rifampin, ED_{50} is the apparent half-inhibitory constant, γ is the sigmoidicity factor, and PR is the potency ratio. This profile maintains a maximum inhibition of P-gp–mediated efflux (of [^{3}H]-verapamil) for both rifampin delivery routes of 62 ± 6%, an ED_{50} of 65 ± 7 mg/kg, and a potency ratio (nasal vs. systemic rifampin) of 417 ± 42. Using the potency ratio, the ED_{50} for nasally administered rifampin was approximately 0.16 mg/kg compared to approximately 65 mg/kg for systemically administered rifampin.

Brain Disposition of [^{3}H]-Verapamil Following Rifampin Administration

In order to investigate the distribution of [^{3}H]-verapamil to different brain regions depending on the route(s) of delivery, brains from individual animals (n = 3) from each experimental group were sliced in sequential 300-μm sections in a rostral-to-caudal direction and examined for [^{3}H]-verapamil content. Figure 6 depicts the brain disposition of [^{3}H]-verapamil following the nasal administration of rifampin. The $AUC_{0\text{-}20}$ (dpm · slice/mg) was increased for systemically administered [^{3}H]-verapamil compared to nasally administered [^{3}H]-verapamil following the nasal instillation of rifampin (365 ± 63 and 276 ± 49 dpm · slice/mg, respectively). It is

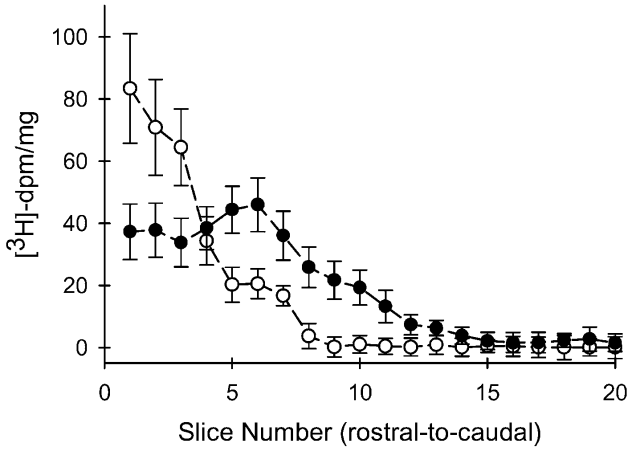

Fig. 6. Representation of the caudal distribution of nasally administered [^{3}H]-verapamil [○, (5 μl, 5 μM, 0.5 mCi/ml)] vs. systemically administered [^{3}H]-verapamil [●, (1 μM; 0.1 μCi/ml; 60s, 2.5 ml/min] following nasal administration of rifampin (10 μl, 1 mM). n = 3.

evident from this figure that when the inhibitor and substrate were both given nasally, there was increased substrate accumulation in the rostral portions of the brain. On the other hand, when the inhibitor was given nasally and the substrate systemically, there was increased caudal penetration compared to the nasal-nasal combination, but the extreme caudal section of the brain evidenced limited substrate uptake. The brain disposition following the systemic delivery of rifampin (Fig. 7) differed markedly from the nasal inhibitor profiles. The $AUC_{0\text{-}20}$ (dpm · slice/mg) was almost 2-fold higher when both the substrate and inhibitor were administered systemically compared to the systemic administration of rifampin followed by the nasal instillation of [^{3}H]-verapamil (478 ± 84 and 268 ± 44 dpm · slice/mg, respectively, $p < 0.01$). There was relatively uniform substrate penetration when both inhibitor and substrate were administered systemically, and the contour of the line follows that of regional blood volumes (12). For instance, the uptake in the striatum and thalamus region (slices 7–10) was lower than in the frontal cortex (slices 3–6). Conversely, when the substrate was administered nasally following the systemic administration of inhibitor, there was increased substrate penetration in the rostral portions of the brain with limited substrate accessing the caudal segments.

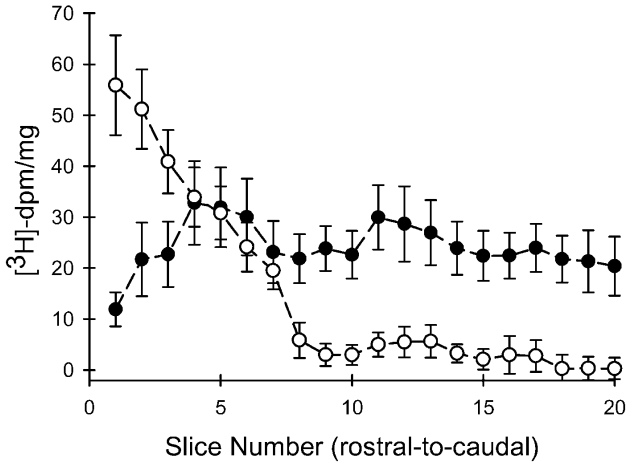

Fig. 7. Representation of the caudal distribution of nasally administered [^{3}H]-verapamil [○, (5 μl, 5 μM, 0.5 mCi/ml)] vs. systemically administered [^{3}H]-verapamil [●, (1 μM; 0.1 μCi/ml; 60s, 2.5 ml/min)] following the systemic administration of rifampin (150 mg/kg). n = 3.

P-glycoprotein Localization

Incubation with anti-P-gp primary antibodies followed by conjugation with fluorochrome-labeled secondary antibodies allowed for the localization of P-gp by laser scanning confocal microscopy. To determine the cellular localization of P-gp, the protein was co-localized with both the endothelial cell marker Glut1 and the epithelial cell marker pan-cytokeratin. In the *mdr1a(+/+)* mice, P-gp was localized to the endothelial cells that line the olfactory bulb (Fig. 8, panels D-F) and the olfactory epithelium (Fig. 8, panels A–C). In the control *mdr1a(–/–)* mice, P-gp was absent in the olfactory epithelium (Fig. 8, panels G–I), and there was no uniform detectable staining for P-gp in the olfactory bulb. As a second negative control, and to confirm the specificity of the secondary antibody, tissue was incubated with rabbit IgG from non-P-gp immunized rabbits followed by fluorochrome conjugated anti-rabbit secondary antibodies. These samples indicated that limited background signal from rabbit IgG (acting as the primary antibody) contributed to the signal for P-gp.

DISCUSSION

It was shown previously that P-gp serves to limit the uptake of substrates delivered by nasal administration, and

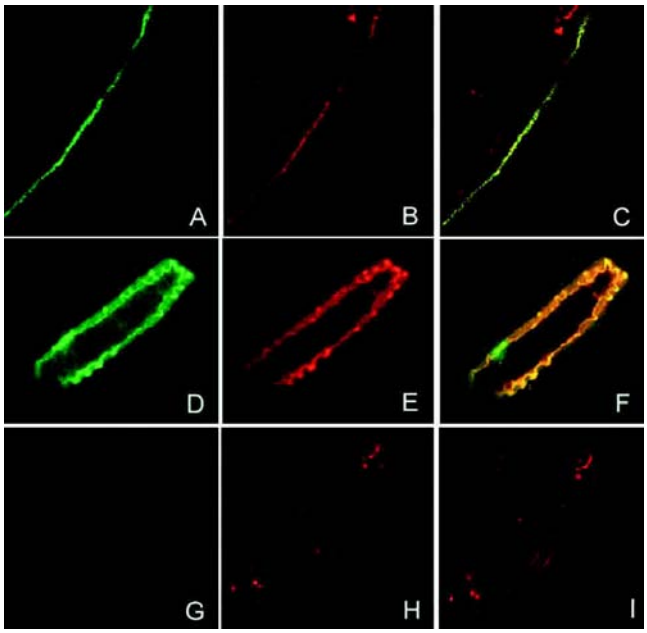

Fig. 8. Immunohistochemical staining for P-glycoprotein in the olfactory epithelium (panels A–C) and the endothelium lining the olfactory bulb (panels D–F). Panel A shows staining for P-gp with C219, panel B shows staining for epithelial cells with pan-cytokeratin, and panel C shows the co-localization of P-gp with the epithelial cells. Panel D shows a representative group of endothelial cells lining the olfactory bulb stained for P-gp (C219), panel E shows staining for endothelial cells with Glut1, and panel F shows the colocalization of P-gp with the endothelial cells of the olfactory bulb. Panels G–I show the negative control for epithelial cell staining using *mdr1a(–/–)* mice. Panel G shows staining for P-gp, panel H shows staining for epithelial cells, and panel I shows the co-localization.

that this attenuation could be overcome by a nasally administered inhibitor (3). However, these studies focused on the whole brain and did not examine compound distribution within the brain following nasal delivery, nor did they address whether the observed effect was simply localized to the olfactory bulb. In addition, these studies did not explore the potential application of transport inhibitor administration via the nasal route to enhance drug uptake across the BBB when the pharmacologic agent is administered by a non-nasal route. Clearly, the ability to deliver modulators of P-gp or other efflux transporters specifically to the brain or BBB, avoiding interaction with these transport proteins in other organs and tissues (e.g., the GI tract, liver), would represent a significant advantage in CNS therapeutics.

The current experiments demonstrated that there are distinct relationships for the different combinations of administration routes for an inhibitor and substrate (nasal vs. systemic). As would be expected, the maximum degree of inhibition was achieved when both the inhibitor and substrate were administered nasally (Fig. 1). The fact that nasal rifampin could abolish the P-gp–mediated transport of nasal [^{3}H]-verapamil is consistent with previous data indicating that at sufficiently high concentrations, rifampin could inhibit completely the P-gp–mediated efflux of verapamil at the BBB (14). This is likely due to the nature of this delivery route, in that both the substrate and inhibitor are exposed to P-gp–mediated efflux equally.

Systemic delivery of rifampin resulted in incomplete inhibition of P-gp–mediated efflux, whether [^{3}H]-verapamil was administered either systemically or nasally (Figs. 3 and 4, respectively). This incomplete inhibition likely is due to an inability to achieve adequate rifampin concentrations at the BBB after systemic administration because of dose-limiting toxicity (150 mg/kg was the highest dose tolerated). This is similar to previous studies which have shown increased brain uptake of substrates in the presence of P-gp inhibitors, but less than complete P-gp inhibition (15).

Despite the fact that inhibition was incomplete, nasal delivery of rifampin resulted in a substantially increased brain uptake of systemically administered [^{3}H]-verapamil (Fig. 2). In fact, the magnitude of P-gp inhibition was comparable to that achieved with systemic rifampin, even though much lower doses were administered nasally. For instance, at a dose equivalent to approximately 0.27 mg/kg, 43.6% inhibition was achieved when the inhibitor was given via the nasal route, compared to 56.2% inhibition when 100 mg/kg rifampin was administered systemically. When comparing the inhibition of P-gp–mediated [^{3}H]-verapamil efflux at the BBB by nasal vs. systemic rifampin, there was an approximate 400-fold lower ED_{50} for nasal compared to systemic rifampin (0.16 vs. 65 mg/kg, respectively, Fig. 5). Thus, theoretically the same % inhibition can be achieved by giving ~400 less dose via nasal administration. Previous studies have indicated that it is the inhibitor concentration in the brain that drives the inhibition of P-gp–mediated transport (14). Thus, the dose advantage observed with nasal rifampin administration is consistent with targeted delivery of rifampin to the brain, resulting in enhanced concentration (of inhibitor) at the BBB compared to systemic rifampin delivery.

An additional experiment that allowed only 7 min to elapse between nasal rifampin instillation and the [^{3}H]-verapamil brain perfusion produced a maximum inhibition of approximately 25.5 ± 6.2%. This obviously was less than the maximum inhibition achieved when 35 min was permitted to elapse between rifampin instillation and [^{3}H]-verapamil perfusion (43.6 ± 8.2%), indicating that the magnitude of transport inhibition is dependent of the dose and route of the inhibitor as well as the time after administration of the inhibitor. This difference in degree of inhibition is likely due to the increased penetration of the nasally administered inhibitor over time. Thus, it is likely that with optimization of this approach, including proper inhibitor selection and dosing schedule for both inhibitor and substrate, improved substrate penetration could be achieved (15).

The pharmacologic implications of utilizing this route of delivery are most likely dependent upon the substrate being able to reach the pharmacologic target. Therefore, it was important to examine the brain distribution, and how distribution might change according to the route(s) of delivery of the inhibitor and/or substrate. It was evident from these experiments that nasal delivery resulted in enhanced delivery to the rostral portion of the brain (Figs. 6 and 7). There was a significant difference in the AUC (dpm · slice/mg) when [^{3}H]-verapamil was delivered nasally (268 ± 44 and 276 ± 49 for systemic vs. nasal rifampin, respectively) vs. systemically (478 ± 84 and 365 ± 63 for systemic vs. nasal rifampin, respectively; $p < 0.01$). However, there was no significant difference in the AUC (dpm · slice/mg) when the rifampin was delivered nasally (276 ± 49 and 365 ± 63 for nasal vs. systemic verapamil, respectively) vs. systemically (268 ± 44 and 478 ± 84 for nasal vs. systemic verapamil, respectively). This indicates that the delivery route of the inhibitor, while important, is not as important as the delivery route of the substrate with regards to enhancing brain uptake. On the other hand, while the overall exposure is comparable between nasal rifampin and systemic rifampin, it is clear from the profiles (Figs. 6 and 7) that there is a distinct advantage for uptake in the rostral portions of the brain when the inhibitor is delivered nasally compared to the more uniform brain disposition following the systemic delivery of the inhibitor. This could have obvious therapeutic implications. The pharmacologic impact of utilizing the nasal route of delivery depends not only enhancing brain uptake, but also on the ability of the substrate to reach its pharmacologic target, which may be problematic with nasal delivery for caudal portions of the brain.

Other studies in our laboratory have indicated that in the absence of transporter-mediated flux, the distribution of compounds in the brain following nasal instillation is diffusional in a rostral-to-caudal direction and is mainly dependent on the lipophilicity of the compound (16). Therefore, it is likely that the degree of inhibition following nasal administration will be higher in the rostral portions of the brain compared to systemic administration of the same inhibitor, assuming that the inhibitor is not a substrate for transport-mediated flux. Moreover, when addressing the brain uptake of subsequent systemic administration of a substrate, the distribution of the substrate within the brain is going to be dependent on the nature of transporter inhibition achieved. Nasal administration of an inhibitor clearly presents a significant degree of inhibition in the rostral portions of the brain and the degree of inhibition decreases toward the more caudal portions, therefore, the uptake of substrate will follow this same pattern (Figs. 6 and 7). On the other hand, systemic administration of an inhibitor will allow a more uniform inhibition

throughout the BBB, and thus the uptake of substrate will follow this same pattern (Figs. 6 and 7).

The immunohistochemical studies reported herein confirm the presence of P-gp at the murine olfactory epithelium, and it is likely that this localization attenuates the delivery of P-gp substrates to the brain. P-gp in the nasal mucosa also likely plays a role in the attenuation of brain uptake of compounds, but the present data imply that nasally delivered substrates are able to access the olfactory epithelium and blood supply in order to modulate BBB P-gp. The olfactory region is primarily supplied with blood from the ophthalmic artery, and there is evidence for a local vascular pathway associated with brain delivery via nasal delivery (17,18). Thus, it is possible that nasally delivered inhibitors are able to access this local blood supply and have an impact on BBB-specific transporters.

There is significant interest in the potential for developing transport inhibitors in order to improve drug delivery specifically to the brain. These efforts have failed, largely due to the systemic toxicity associated with these inhibitors. Nasal delivery of transport-specific inhibitors appears to offer a means to inhibit efflux transport at the BBB while maintaining low systemic concentrations of the inhibitor (thus limiting systemic toxicity). The magnitude of this transport inhibition is dependent on the dose and the route of the inhibitor, the time after administration of the inhibitor, and the specific brain region examined. In addition, it should be taken into account that this approach is only viable if the toxicity associated with a specific inhibitor is not CNS-mediated. Therefore, the potential use of nasal instillation as a way to target transport inhibitors to the brain may serve to enhance the efficacy of inhibitors that have been formulated for delivery via traditional routes.

ACKNOWLEDGMENT

The authors would like to thank C. Robert Bagnell, Ph.D., for his assistance with the immunohistochemistry studies.

REFERENCES

1. C. L. Graff and G. M. Pollack. Drug transport at the blood-brain barrier and the choroid plexus. *Curr. Drug Metab.* **5**:95–108 (2004).
2. R. Polt, F. Porreca, L. Z. Szabo, E. J. Bilsky, P. Davis, T. J. Abbruscato, T. P. Davis, R. Horvath, H. I. Yamamura, and V. J. Hruby. Glycopeptide enkephalin analogues produce analgesia in mice: Evidence for penetration of the blood-brain barrier. *Proc. Natl. Acad. Sci. USA* **91**:7114–7118 (1994).
3. C. L. Graff and G. M. Pollack. P-glycoprotein attenuates brain uptake of substrates after nasal instillation. *Pharm. Res.* **20**:1225–1230 (2003).
4. I. Manzini and D. Schild. Multidrug resistance transporters in the olfactory receptor neurons of Xenopus laevis tadpoles. *J. Physiol.* **546**:375–385 (2003).
5. K. K. Kandimalla and M. D. Donovan. Carrier mediated transport of small molecules across bovine olfactory mucosa: implications in nose to brain transport. *AAPS PharmSci* **5**:T3140 (2003).
6. M. A. Wioland, J. Fleury-Feith, P. Corlieu, F. Commo, G. Monceaux, J. Lacau-St-Guily, and J. F. Bernaudin. CFTR, MDR1, and MRP1 immunolocalization in normal human nasal respiratory mucosa. *J. Histochem. Cytochem.* **48**:1215–1222 (2000).
7. P. Kwan, G. J. Sills, E. Butler, T. W. Gant, and M. J. Brodie. Differential expression of multidrug resistance genes in naive rat brain. *Neurosci. Lett.* **339**:33–36 (2003).
8. J. H. Lin. Drug-drug interaction mediated by inhibition and induction of P-glycoprotein. *Adv. Drug Deliv. Rev.* **55**:53–81 (2003).
9. J. W. Smit, M. T. Huisman, O. van Tellingen, H. R. Wiltshire, and A. H. Schinkel. Absence or pharmacological blocking of placental P-glycoprotein profoundly increases fetal drug exposure. *J. Clin. Invest.* **104**:1441–1447 (1999).
10. U. Mayer, E. Wagenaar, B. Dorobek, J. H. Beijnen, P. Borst, and A. H. Schinkel. Full blockade of intestinal P-glycoprotein and extensive inhibition of blood-brain barrier P-glycoprotein by oral treatment of mice with PSC833. *J. Clin. Invest.* **100**:2430–2436 (1997).
11. J. van Asperen, O. van Tellingen, F. Tijssen, A. H. Schinkel, and J. H. Beijnen. Increased accumulation of doxorubicin and doxorubicinol in cardiac tissue of mice lacking mdr1a P-glycoprotein. *Br. J. Cancer* **79**:108–113 (1999).
12. C. Dagenais, C. Rousselle, G. M. Pollack, and J. M. Scherrmann. Development of an in situ mouse brain perfusion model and its application to mdr1a P-glycoprotein-deficient mice. *J. Cereb. Blood Flow Metab.* **20**:381–386 (2000).
13. Q. R. Smith. *Brain Perfusion Systems for Studies of Drug Uptake and Metabolism in the Central Nervous System*. Plenum Press, New York, 1996.
14. J. Zong and G. M. Pollack. Modulation of P-glycoprotein transport activity in the mouse blood-brain barrier by rifampin. *J. Pharmacol. Exp. Ther.* **306**:556–562 (2003).
15. E. M. Kemper, A. E. van Zandbergen, C. Cleypool, H. A. Mos, W. Boogerd, J. H. Beijnen, and O. van Tellingen. Increased penetration of paclitaxel into the brain by inhibition of P-glycoprotein. *Clin. Cancer Res.* **9**:2849–2855 (2003).
16. C. L. Graff, R. Zhao, and G. M. Pollack. Pharmacokinetics of substrate uptake and distribution in murine brain after nasal instillation. *Pharm. Res.* (in press).
17. J. Skipor, W. Grzegorzewski, N. Einer-Jensen, and B. Wasowska. Local vascular pathway for progesterone transfer to the brain after nasal administration in gilts. *Reprod. Biol.* **3**:143–159 (2003).
18. L. Illum. Transport of drugs from the nasal cavity to the central nervous system. *Eur. J. Pharm. Sci.* **11**:1–18 (2000).